Annals of DAAAM for 2012 & Proceedings of the 23rd International DAAAM Symposium, Volume 23, No.1, ISSN 2304-1382
ISBN 978-3-901509-91-9, CDROM version, Ed. B. Katalinic, Published by DAAAM International, Vienna, Austria, EU, 2012
*Make Harmony between Technology and Nature, and Your Mind will Fly Free as a Bird*
*Annals & Proceedings of DAAAM International 2012*

# HIGH-TEMPERATURE CHLORINE CORROSION IN PRESENCE OF SULFUR-CONTAINING AND POTASSIUM EXTERNAL DEPOSITS

**PRISS, J[elena]; KLEVTSOV, I[van] & WINKELMANN, H[orst]**

***Abstract:*** *The high-temperature corrosion resistance of several boiler steels which are used in a Estonian Power Plants were tested experimentally in laboratory. The aggressive conditions from the real system of high-temperature chlorine corrosion in the presence of sulfur-containing and potassium external deposit were simulated in a High-temperature Corrosion Tester. The recently developed device allows testing in oxidizing and corrosive atmospheres of high temperatures. Experiments were done at temperature 500$^0$C in combination with oil shale ash.*
*Scanning electron microscopy (SEM) and energy dispersive X-Ray spectroscopy (EDX) analysis were carried out to study corrosion products.*
***Keywords****:Oil shale ash, chlorine corrosion, CFB boiler, high-resisting steel, X-ray analysis*

## 1. INTRODUCTION

The high-temperature corrosion resistance of several boiler steels (austenitic X12CrNiTi18-9 alloy,beinitX10CrMoVNb9-1 alloy, perlitic13CrMoV42 alloy, austenitic TP347HFG alloy) which are used in a Estonian Power Plants were tested experimentally in laboratory. The recently developed device allows testing in corrosive atmospheres of high temperatures. Experiments were done at temperature 500$^0$C in combination with Estonian oil shale ash. Oxidation tests at 500$^0$Cwere done in furnace with continuous air flow, to compare results with mass loss during corrosion tests.

## 2. CIRCULATING FLUIDIZED BED BOILER

Estonian oil shale is a complex fossil fuel and processing is difficult. In the circulating fluidized bed (CFB) (Fig. 1)boiler process inorganic matter produces several chemically active compounds leading to fouling and accelerated high-temperature heating surfaces which further accelerates the corrosion process [1]. This occurs mainly due to presence of potassium chloride (KCl) [8].

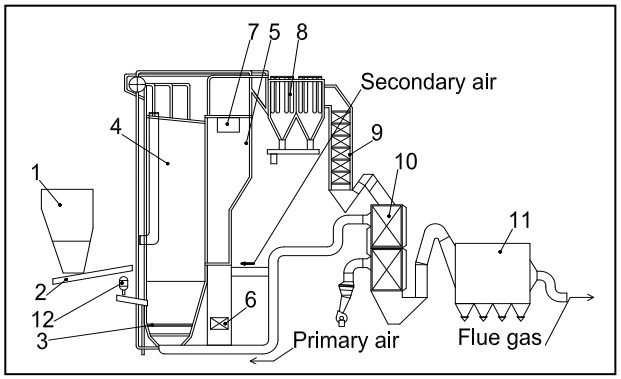


Fig. 1. Oil shale-fired CFB boiler (sample parts). 1-Raw fuel silo, 2-Fuel feeder, 3- Grate, 4- Furnace chamber, 5- Separating chamber, 6-Fluidised bed internal heat exchange (Interex), 7- Separator of solids, 8-Convective superheater and reheater, 9- Economizer, 10- Air preheater, 11- Electrical precipitator, 12- Secondary fuel crusher.

The tubes of superheater and reheater of oil shale steam boilers are subject to intensive corrosion. Metal damage due to high temperature corrosion (HTC) is much higher than creep damage. It is therefore highly significant in condition assessment of the metal of steam boilers heating surfaces to take into account the metal loss due to HTC [5].

In the following subitems the effects of high temperature corrosion and oxidation of the investigated steels are shown and discussed.

This work main objective is to evaluate resistance of selected heat-resisting steel to high-temperature corrosion in an oxidizing atmosphere containing chlorine in presence of potassium (K). The experiments attempt to simulate aggressive conditions of high-temperature chlorine corrosion for optimized material selection.

## 3. MATERIALS CHARACTERIZATION

### 3.1 Steel characterization

The characterization of microstructure has been done with optical microscopy (Leica MEF4A) after etching. Typical microstructures are shown in Fig. 2.

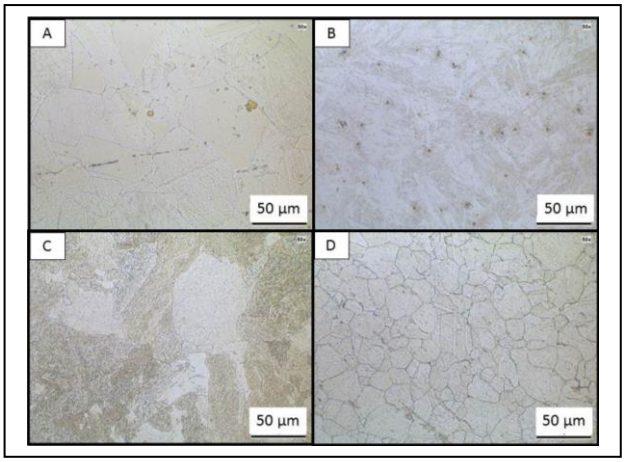


Fig. 2. Microstructures of the investigated materials: (A) austenitic X12CrNiTi18-9 alloy, (B) beinit X10CrMoVNb9-1 alloy, (C) perlitic13CrMoV42 alloy, (D) austenitic TP347HFG alloy

The austenitic steel X12CrNiTi18-9 (A) has a heat resistant microstructure at a cromium (Cr) content of 18% and 10% of nickel (Ni). Austenitic stainless steels have high corrosion resistant because of the alloying elements allow the formation of a passivating layer.

Titanium (Ti) (0.52%) is used for prevention a fracture on the sides of grain.

Adding titanium (Ti) helps to stabilize carbon. It forms titanium carbides and reduces the amount of carbon available to form chromium carbides which is deleterious for corrosion resistance. The addition of nickel will provide improved resistance in reducing environments and to stress corrosion cracking.

Beinit alloy X10CrMoVNb9-1 (B) has microstructure at cromium (Cr) content of 9%. Molybdenum (Mo) (1.08%) is extremely effective in improving pitting and crevice corrosion resistance.

The perlitic steel 13CrMoV42 (C) has cromium (Cr) content of 1.44%.

The austenitic steel TP347HFG (D) has heterogeneous structure in which different grain size can be seen.

Chemical composition of steels investigated in wt. % with (XL30 ESEM-FEG Genesis Spectrum Version 5.11 EDAX Inc.) and are :

1. (A) X12CrNiTi18-9 (DIN 17440) /12X18H10T (GOST 5632-72): Fe= 66,77%; C=0,12%; Si=0,83%; Mn=0%, Cr=18,48%; Ni=10,39%, V=0%; Mo=0%; Ti=0,52%.
2. (B) X10CrMoVNb9-1 (EN 10216-2)/ 18Х12ВМБФР(1583-93): Fe= 89,09%; C=0,12%; Si=0,40%; Mn=0%, Cr=8,86%; Ni=0%, V=0,37%; Mo=1,08%; Nb=0,21%.
3. (C) 13CrMoV42 (DIN 17155)/: Fe= 95,10%; C=0,15%; Si=0,46%; Mn=1,01%, Cr=1,44%; Ni=0,39%, V=0,38%; Mo=1,23%.
4. (D) TP347HFG (EN 10216-5): Fe= 66,16%; C=0,1%; Si=0,66%; Mn=1,98%, Cr=18,64%; Ni=11,19%, V=0%; Mo=0%; Nb=1,37%.

### 3.2 Estonian oil shale ash

Electrical precipitator oil shale ash Fig. 1 (11) with particle size 45-60 μm from Narva Power Plant from circulating fluidized bed (CFB) boiler was used in laboratory experiment in corrosion test.

Chemical composition of Estonian oil shale ash: $CO_2$=5,11%; $C_{elem}(CO_2)$=1,37% (5,04%); $SO_{3common}(S_{com})$=1,86%; $S_{sulfiid}$=0%; $SiO_2$=35,7%;$Fe_2O_3$=5,33%; $Al_2O_3$=8,47%; $CaO_v$=10,8%; CaO=29,4%; MgO=5,63%; $K_2O$=4,1%; $Na_2O$=0,25%; Cl=0,5%; unburned parts=5,6%. Chemical composition was measured by wet chemistry analysis method.

The fusion temperatures of ash depend on the chemical and mineralogical composition of the ash. The main components in oil shale ash that influence ash fusibility are CaO, $SiO_2$ and $Al_2O_3$. Oil shale mineral matter is a heterogeneous system containing minerals of carbonate and sandy-clay parts. Therefore, different ash particles have different fusion temperatures depending on the proportions of the mentioned components [2].

The fusion temperature for oil shale ash different components is higher than 1000 $^0$C [8].

## 4. CORROSION EXPERIMENTAL

The corrosion tests were carried out at four steels (X12CrNiTi18-9, X10CrMoVNb9-1, 13CrMoV42, TP347HFG ) in new high temperature corrosion tester (Fig. 3) at the „Austrian Excellence Centre for Tribology“ ($AC^2T$). The experiments were done at 500$^0$C with 24h exposure time in a horizontal furnace equipped with a ceramic working tube (Fig. 4). The corrosion tests have been performed on grinded specimens (25x15x6 mm), which have been cut from original boiler tubes.Prior to the tests all specimens were ultrasonically cleaned and degreased with ethanol, precisely measured and weighed and after that samples were coated manually by brush with mixture of oil shale ash and ethanol alcohol ($C_2H_5OH$) for imitation of oil shale ash on-tube deposits for the corrosion test.

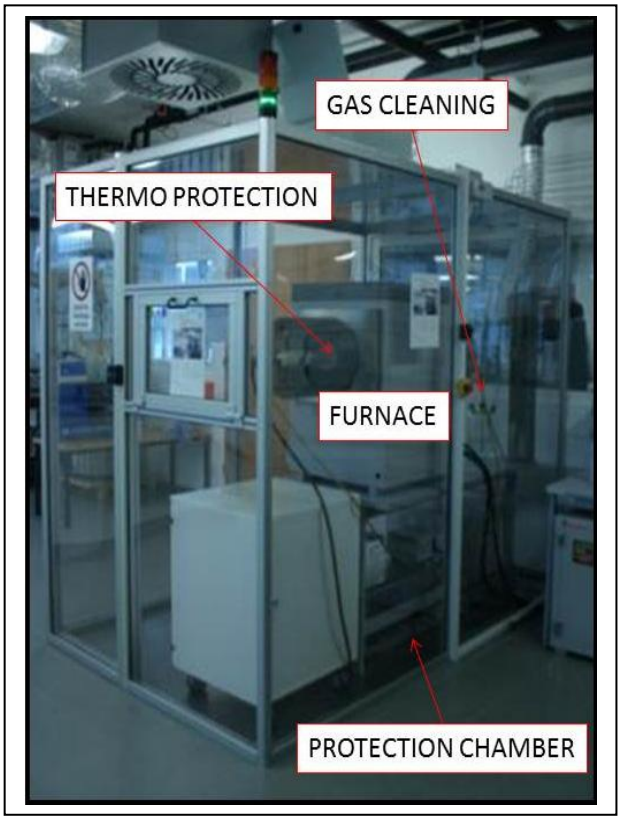

Fig. 3. The high temperature corrosion (HTC) tester illustration.

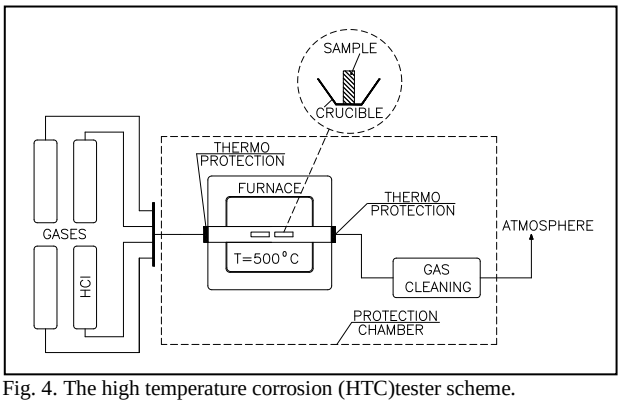

Fig. 4. The high temperature corrosion (HTC)tester scheme.

Schematic illustration of high temperature corrosion (HTC) tester where selected steels were tested is presented in Fig. 4.

The exposures were carried out in temperature-controlled horizontal tube furnace. For the experiments under corrosion environment the gas (HCl) was passed through a chamber (with a velocity of 0,019 m/s). The samples were positioned vertically, parallel to the flow direction.

After the procedure the samples were weighed. Not to remove corrosion layer after the test, samples were grinded with oil, for SEM preparation.

## 5. OXIDATIONEXPERIMENTAL

Steel oxidation rates in $O_2$ or air are taken as the basis for comparison with other, more aggressive forms of corrosion.

For the experiments under oxidation environment, the samples were put in furnace at $500^0$C with 24hin synthetic air atmosphere ($O_2$~20%, $N_2$~80%). The oxidation test have been performed on grinded specimens, ultrasonically cleaned and degreased with ethanol. The characterization of the oxidation was studied quantitatively by mass change of materials.

## 6. HOT CORROSION AND OXIDATION STUDIES

High-temperature corrosion in an atmosphere containing chlorine is complex. It leads to the formation of scale with an exemplary structure presented in Fig.5. Incase of low alloy heat-resisting steels, the scale in two of its first layers consist iron, hematite and magnetite oxides and in the bottom layer, there are iron chlorides and sulfides. In high alloy heat-resisting steels the structure of scale is similar, however, in the bottom layer, double chromic and ferric oxides (spinels) may occur [3].

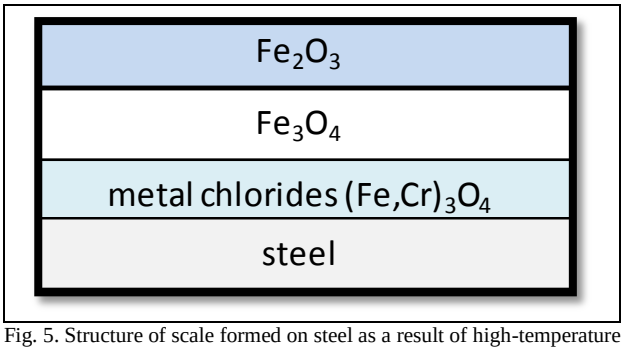


Fig. 5. Structure of scale formed on steel as a result of high-temperature chlorine corrosion.

## 7. CORROSION AND OXIDATION BEHAVIOR

In the following subitem the effects of high temperature corrosion and oxidation of the investigated steels are shown and discussed. Quantitative and qualitative analyses were performed to understand high temperature corrosion of the presented materials. Determination of mass changes and their comparison to different effects which took place during the thermal treatment in corrosive and oxidation media were made as well.

In addition qualitative analysis were performed with scanning electron microscope (ZEISS FESEM GEMINI SUPRA VP) and energy dispersive X-Ray spectroscopy (EDS-EBSD) analysis were performed. Metallographic cross sections of the corroded samples were prepared to analyse formed layers and the corrosive behavior of different phases from all materials investigated.

Fig. 6 presents SEM cross-sectional analysis of the materials investigated. The oxide layer formed after 500 $^0$C corrosion test for 24h is different for austenitic, perlitic and beinit alloys: (A) austenitic X12CrNiTi18-9 alloy ~5 μm; (B)beinit X10CrMoVNb9-1 alloy~0 μm;(C)perlitic13CrMoV42 alloy~0 μm; (D)austenitic TP347HFG alloy~4 μm.

As it was mentioned oxide layer thickness depends on chemical composition of materials. Materials (A) austenitic X12CrNiTi18-9 alloy and (D)austenitic TP347HFG alloyconsist 18.48% and 18.64 % of chromium (Cr), 10.39% and 11.19% of nickel (Ni). In present experiment alloying elements in materials (A) and (D) produced protective layers. Due to diffusion corrosive molten salts are generated below the protective layer (Fig. 9) and (Fig. 18).

Material (B)beinit X10CrMoVNb9-1 alloyconsist only 8.86% of chromium (Cr)and 1.08% ofmolybdenum (Mn).Result oxides of iron (Fe) produced high mass changes(Fig. 7) during corrosion test.

Material (C)perlitic13CrMoV42 alloy has not generate any protective layer, because of low alloy heat-resisting steelsproperties, chromium (Cr) content only 1,44%.

The comparison of materials (A) austenitic X12CrNiTi18-9 alloy and (D)austenitic TP347HFG alloy investigated, as seen in Fig. 9 shows good stability against oxidation at $500^0$C. Material (B)beinit X10CrMoVNb9-1 alloy and (C)perlitic13CrMoV42 alloy arelow alloy heat-resisting steels and the result against oxidationat $500^0$C are conformable.

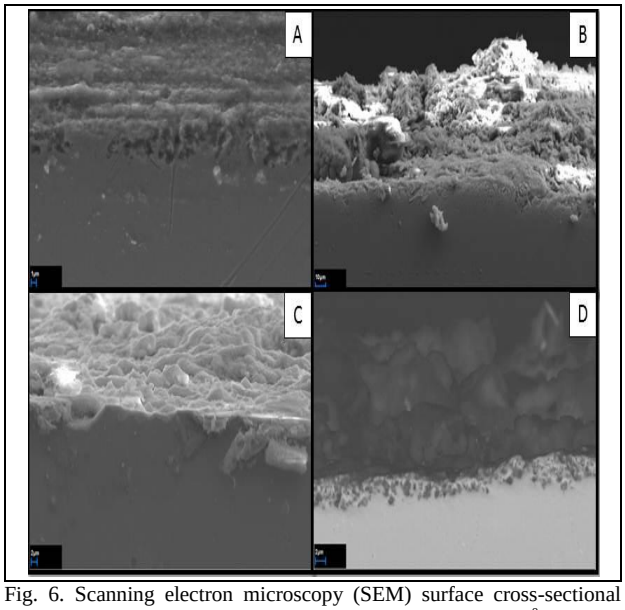


Fig. 6. Scanning electron microscopy (SEM) surface cross-sectional analysis of the oxide layer formed after corrosion tests at $500^0$C for 24h on materials: (A) austenitic X12CrNiTi18-9 alloy, (B)beinit X10CrMoVNb9-1 alloy, (C) perlitic13CrMoV42alloy, (D) austenitic TP347HFG alloy.

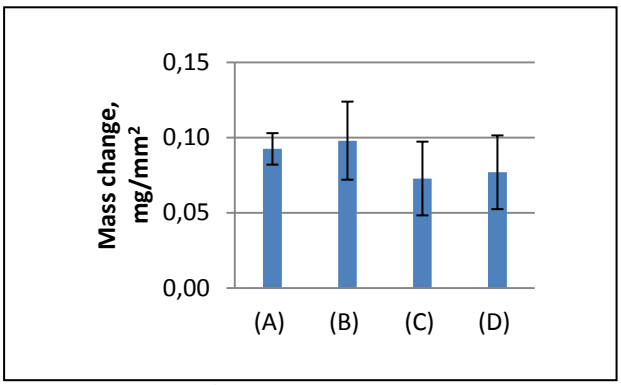


Fig. 7. Mass changes of the materials investigated under corrosion at 500$^0$C for 24h on materials:.(A)austenitic X12CrNiTi18-9 alloy, (B)beinit X10CrMoVNb9-1 alloy, (C) perlitic 13CrMoV42 alloy, (D) austenitic TP347HFG alloy.

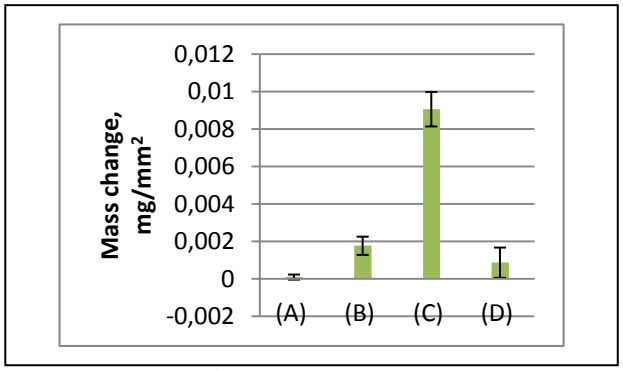


Fig. 8. Mass changes of the materials investigated under oxidation at 500$^0$C for 24h on materials:.(A)austenitic X12CrNiTi18-9 alloy, (B)beinit X10CrMoVNb9-1 alloy, (C) perlitic 13CrMoV42 alloy, (D) austenitic TP347HFG alloy.

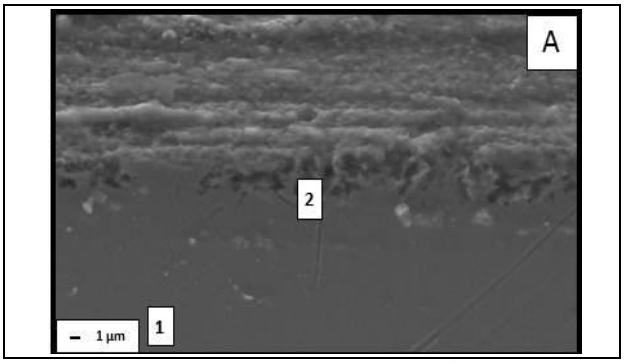


Fig. 9. Scanning electron microscopy (SEM) surface cross-sectional analysis after corrosion tests at 500$^0$C for 24h for material (A)austenitic X12CrNiTi18-9alloy.

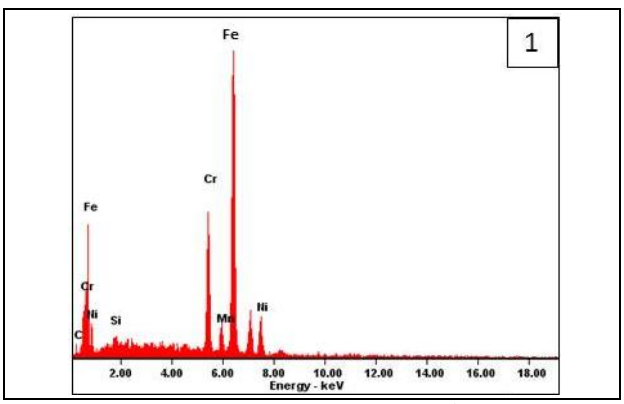


Fig. 10. Scanning electron microscopy (SEM) surface cross-sectional analysis region (1) after corrosion tests at 500$^0$C for 24h for material (A) austenitic X12CrNiTi18-9alloy.

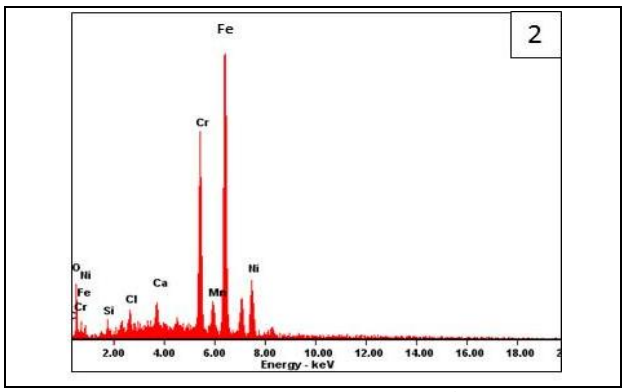


Fig. 11. Scanning electron microscopy (SEM) surface cross-sectional analysis region (2) after corrosion tests at 500$^0$C for 24h for material (A)austenitic X12CrNiTi18-9alloy.

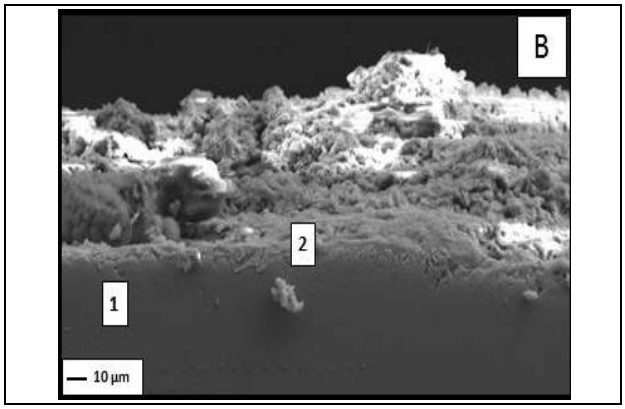


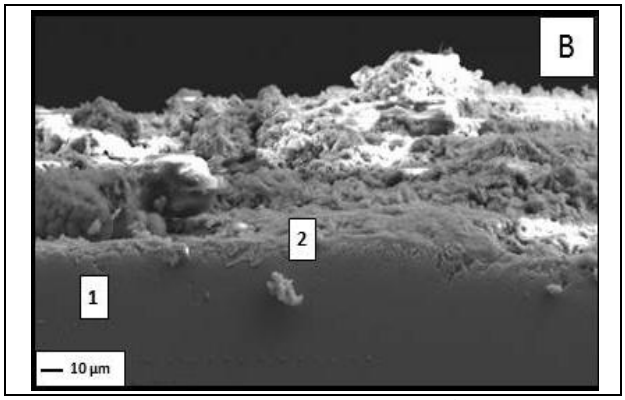


Fig. 12. Scanning electron microscopy (SEM) surface cross-sectional analysis after corrosion tests at 500$^0$C for 24h for material (B) beinit X10CrMoVNb9-1 alloy.

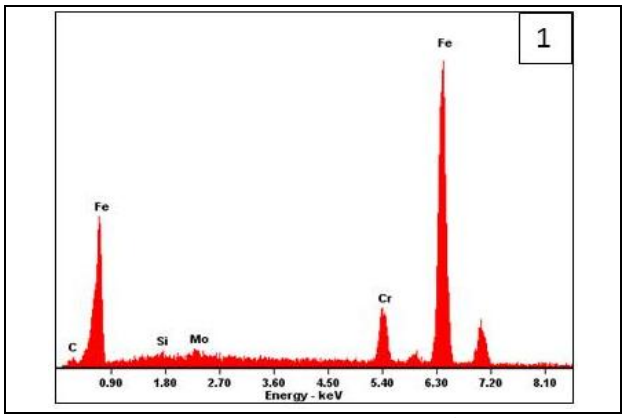


Fig. 13. Scanning electron microscopy (SEM) surface cross-sectional analysisregion (1) after corrosion tests at 500$^0$C for 24h for material (B) beinit X10CrMoVNb9-1 alloy.

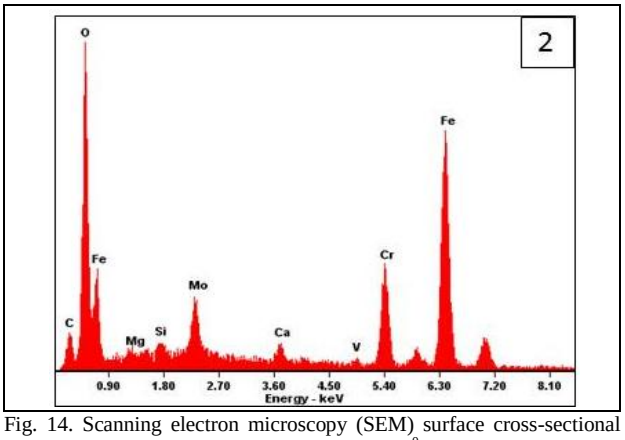


Fig. 14. Scanning electron microscopy (SEM) surface cross-sectional analysisregion (2) after corrosion tests at $500^0$C for 24h for material (B)beinit X10CrMoVNb9-1 alloy.

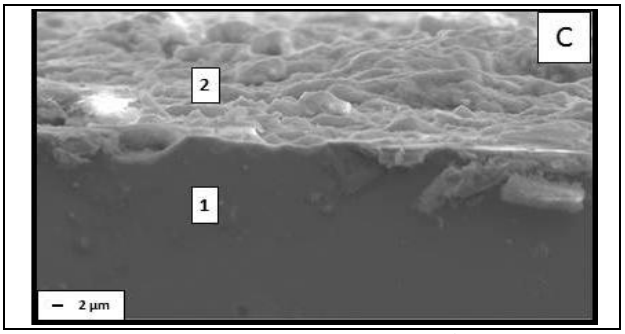


Fig. 15. Scanning electron microscopy (SEM) surface cross-sectional analysis after corrosion tests at $500^0$C for 24h for material (C) perlitic 13CrMoV42 alloy.

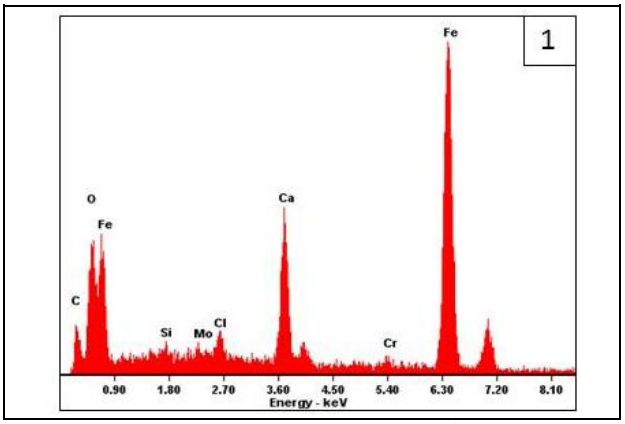


Fig. 16. Scanning electron microscopy (SEM) surface cross-sectional analysisregion (1) after corrosion tests at $500^0$C for 24h for material (C) perlitic13CrMoV42 alloy.

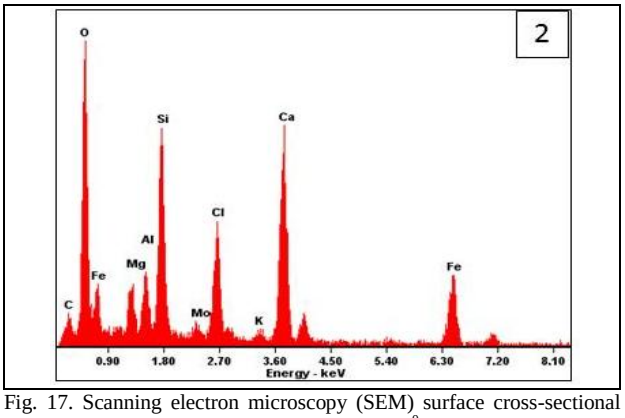


Fig. 17. Scanning electron microscopy (SEM) surface cross-sectional analysisregion (2) after corrosion tests at $500^0$C for 24h for material (C)perlitic13CrMoV42alloy.

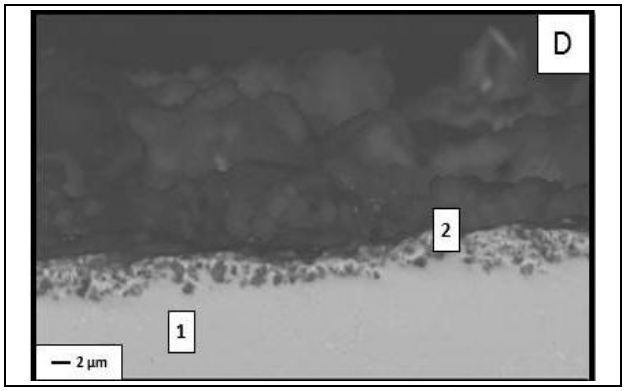


Fig. 18. Scanning electron microscopy (SEM) surface cross-sectional analysis after corrosion tests at $500^0$C for 24h for material (D)austenitic TP347HFG alloy.

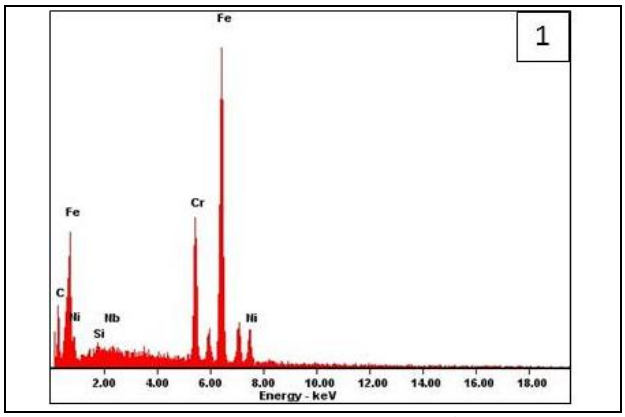


Fig. 19. Scanning electron microscopy (SEM) surface cross-sectional analysisregion (1) after corrosion tests at $500^0$C for 24h for material (D) austenitic TP347HFG alloy.

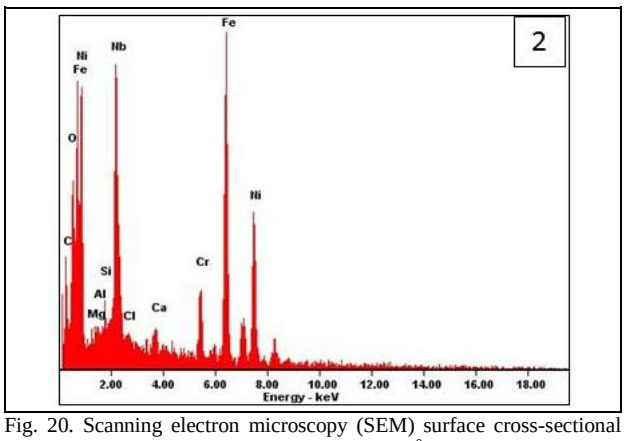


Fig. 20. Scanning electron microscopy (SEM) surface cross-sectional analysis region (2) after corrosion tests at $500^0$C for 24h for material (D)austenitic TP347HFG alloy.

## 8. CORROSION MECHANISMS

In the present experiment hot corrosion involves reactions between molten salt and the alloy undergoing oxidation. Ideally, in a "clean" environment like air, the normal oxide film which forms at the surface of an alloy acts as an effective barrier to further oxidation. The continuing growth of the oxide film requires the transport of metal species or oxidant species through the film via solid diffusion. In practice, however, the oxide film often becomes porous and cracked, allowing much faster transport along these channels and leading to heterogeneous film morphology. Transport is typically the rate-limiting step, and therefore steady state

conditions establish a gradient in oxygen activity across the scale. When molten salt is also present, the salt wets the surfaces of the oxides and is able to penetrate into and through the pores and cracks by capillary action. Since transport via diffusion through the molten salt will be much faster than via solid state diffusion through the oxide scale, the scale will grow much faster, and the relevant gradients and chemical reactions will be those involving salt, scale and metal phases [7].

In presented corrosion experiment no oxygen ($O_2$) was added into the gas flow, pure hydrogen chlorine (HCl) was reacted with steels covered with oil shale ash. The reaction with gas (HCl) and ash, containing sulfides leads to salts formation. Under high temperature melting salts produced localized molten salts corrosion. Explanation of scale and corrosion mechanisms is present in Fig. 21.

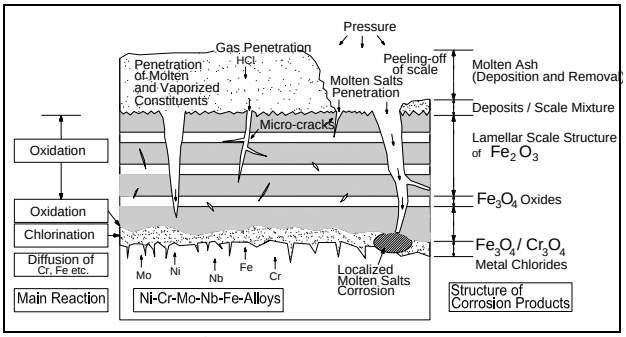


Fig. 21. Explanation of scale and corrosion mechanisms in Ni-Cr-Mo-Nb-Fe alloys.

## 9. CONCLUSION

As expected investigated austenitic steels (A) X12CrNiTi18-9 and (D)TP347HFG show good stability against oxidation, in comparison tomaterials (B) X10CrMoVNb9-1 beinit and (C)13CrMoV42 perlit.

Usually high temperature chlorine corrosion resistance of steels depends on chromium contents.However, in this case the scale on the investigated heat-resisting steels is characterized by a multilayer structure.

Under test conditions, the investigated austenitic steels (A) X12CrNiTi18-9 and (D) TP347HFG showfaster scale grow, because transport via diffusion through molten salt is faster than via solid state diffusion through an oxide scale.

As a resultin presence of sulfur-containing and potassium external deposits corrosion resistance is better than expected for (B) X10CrMoVNb9-1,beinitand (C) 13CrMoV42perliticsteels, in comparison to the tested austenitic alloys (A) X12CrNiTi18-9 and (D) TP347HFG.

The corrosion tests were carried out at four steels in new high temperature corrosion tester at the „Austrian Excellence Centre for Tribology“ ($AC^2T$). The experiments were done at $500^0$C with 24h exposure time in combination with Estonian oil shale ash.

In future plans is to make the tests for the same steels in mixed gases atmosphere ($CO_2$, $SO_2$, HCl) at temperatures $500^0$C and $600^0$C. Experiments with different temperatures will allow to make comparable analysis.

## 10. ACKNOWLEDGEMENTS

This work was funded by the „ESF DoRa T6“ (Development of International cooperation networks by supporting the mobility of Estonian doctoral students) and has been carried out within the „Austrian Excellence Centre for Tribology“ ($AC^2T$ research GmbH). The authours are also grateful to Department of Thermal Engineering (Tallinn University of Technology) for supplying starting materials. Ms. Christian Katsich, Mr. CristophMozelt and Mr. Markus Flasch from $AC^2T$ for cooperation and Bc. StenVinogradov from Tallinn University of Technology for operating High temperature corrosion tester.

## 11. REFERENCES

[1] Klevtsov, I.; Tallermo, H.& Bojarinova, T. (2005) High temperature corrosion of boiler steels munder chlorine-containing surfake deposits, *Journal of pressure vessel technology*. Vol.127

[2] Ots.A.(2007). Estonian oil shale properties and utilization in power plants. *Energetika*, Vol.53, Nr.2, 8-18

[3] Hernas, A., Imosa, M., Formanek, B. & Cizner.J. (2004) High-temperature chlorine-sulfur corrosion of heat-resisting steels“. *Journal of Materials Processing Technology*. 157-158. pp. 348-353

[4] Plamus. K.. (2012). The Impact of Oil Shale Calorific Value on CFB Boiler Thermal Efficiency and Environment. Ph.D. Dissertation, Department of Thermal Engineering, Tallinn University of Technology, Tallinn, Estonia

[5] Dedov. A. (2007). Assessment of Metal Condition and Remaining Life of In-service Power Plant Components Operating at High Temperature. Ph.D. Dissertation, Department of Thermal Engineering, Tallinn University of Technology, Tallinn, Estonia

[6] J.Lehmusto, J. (2012). High temperature corrosion of superheater steels by KCl and K2CO3 under dry and wet conditions“, *Fuel processing Technology*. doi: 10.1016/j.fuproc.2012.05.020

[7] Shores.D.A., Mohanty. B.P.(2004). Role of chlorides in hot corrosion of a cast Fe-Cr-Ni alloy. Part II: thermochemical model studies. *Corrosion science*, Vol.46, 2909-2924

[8] Ots, A., (2005*). Oil Shale Combustion Technology*. Tallinn, ISBN 9985-894-74-X